LA-UR- 97 - 1772

CONF-970503--238

Approved for public release; distribution is unlimited.

Title: ALGORITHMS AND IMPLEMENTATIONS OF APT RESONANT CONTROL SYSTEM

Author(s): YI-MING WANG, LANSCE-5
AMY REGAN, LANSCE-5

Submitted to: PARTICLE ACCELERATOR CONFERENCE 1997
VANCOUVER, BRITISH COLUMBIA, CANADA
MAY 12-16, 1997

DISCLAIMER

Los Alamos
NATIONAL LABORATORY

Los Alamos National Laboratory, an affirmative action/equal opportunity employer, is operated by the University of California for the U.S. Department of Energy under contract W-7405-ENG-36. By acceptance of this article, the publisher recognizes that the U.S. Government retains a nonexclusive, royalty-free license to publish or reproduce the published form of this contribution, or to allow others to do so, for U.S. Government purposes. Los Alamos National Laboratory requests that the publisher identify this article as work performed under the auspices of the U.S. Department of Energy. The Los Alamos National Laboratory strongly supports academic freedom and a researcher's right to publish; as an institution, however, the Laboratory does not endorse the viewpoint of a publication or guarantee its technical correctness.

Form 836 (10/96)

ALGORITHMS AND IMPLEMENTATIONS OF APT RESONANT CONTROL SYSTEM*

Yi-Ming Wang† and Amy Regan, Los Alamos National Laboratory,
P.O. Box 1663, Los Alamos, NM 87545, USA

Abstract

A digital signal processor is implemented to control resonant frequency of the RFQ prototype in APT/LEDA. Two schemes are implemented to calculate the resonant frequency of RFQ. One uses the measurement of the forward and reflected fields. The other uses the measurement of the forward and transmitted fields. The former is sensitive and accurate when the operation frequency is relatively far from the resonant frequency. The latter gives accurate results when the operation frequency is close to the resonant frequency. Linearized algorithms are derived to calculate the resonant frequency of the RFQ efficiently using a fixed-point DSP. The control frequency range is about 100kHz for 350MHz operation frequency. A frequency agile scheme is employed using a dual direct digital synthesizer to drive the klystron at the cavity's resonant frequency (not necessarily the required beam resonant frequency) in power-up mode to quickly the cavity to the desired resonant frequency. This paper will address the algorithm implementation, error analysis, as well as related hardware design issues.

1 INTRODUCTION

Resonant control of RFQ and superdonducting RF cavities requires accurate measurement of resonant frequency of RF cavities. For a digital implementation of the resonant control system in APT/LEDA, an efficient and accurate algorithm is needed to provide a real time error signal to water cooling system within a desired bandwidth. The algorithm proposed in this paper utilizes the vector measurement of the forward, reflected, and transmitted fields to calculate the complex load impedance or admittance. Knowing the complex load impedance and the loaded quality factor Q of the cavity, the discrepancy of the operating frequency and the resonant frequency can be derived accordingly. A simple linear relation between the imaginary part of load admittance and error signal (difference between operating frequency and the resonant frequency of RF cavity) is derived by linearizing a general quadratic relation between the imaginary load admittance and resonant frequency. The numerical simulations reveal that the difference between the full solution and approximated linear solution is neglect within the frequency range we are interested ($f_0 \pm 100$Hz).

2 SYSTEM IMPLEMENTATION

Figure 1 is a block diagram of the resonant control module for APT/LEDA.

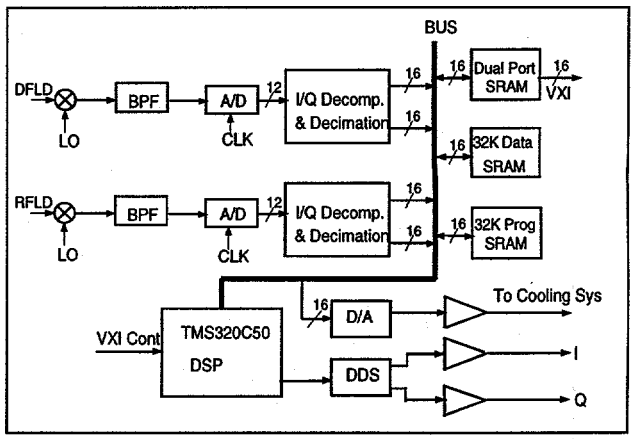

Figure 1. Block Diagram of Resonant Control Module

The RF frequency is 350MHz for APT/LEDA. The LO is 300MHz. The clock for A/D converter is 40Mhz. Since the IF frequency is 50MHz, the output of the A/D converter is a data steam consisting of the repeat pattern of measurement of I, Q, -I, and -Q components. The output of the A/D converter is fed into a multiplexer that switches every other samples into two parallel paths to separate the I and Q components. Then, each channel of data steam is multiplied by +1 and -1 alternately to remove the sign alternate inversion in the corresponding data steam. The outputs are the measured I and Q components of the input RF signal. The major advantage of the above described digital I/Q demodulation scheme is the single analog signal path for both I and Q components which insures a perfect gain-matching between the I and Q signals. Secondly, since the sampled signal is at the IF frequency which is 50MHz in our case, analog DC offsets and drifts do not affect the accuracy of the digital I/Q demodulation. A dual DDS (direct digital synthesizer) is used to generate two off-phase error correction sine waves for I/Q modulation in the frequency agile mode.

* Work supported by US Department of Energy.

3 RESONANT CONTROL ALGORITHM

The resonant control algorithm of APT/LEDA is based on the vector measurement of the forward, reflected or transmitted fields. Figure 2 depicted a simplified transmission model for a cavity driving system. The complex load impedance of the cavity is Z_L. The transmission line impedance is Z_0. The forward and reflected field are measured at z_1 and z_2 respectively, which are between $z=0$ and $z=l$. Here l is the length of the transmission line from klystron to cavity.

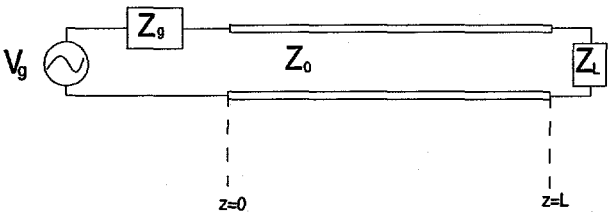

Figure 2. Waveguide with a length of L and load Z_L.

With $e^{j\omega}$ convention, the field in the transmission line can be expressed as

$$V(z) = V_0^+ e^{-z\gamma} + V_0^- e^{z\gamma} \quad (1)$$

$$I(z) = I_0^+ e^{-z\gamma} + I_0^- e^{z\gamma} \quad (2)$$

where,

$\gamma = \alpha + j\beta$

V_0^+, I_0^+ stand for the incident field

V_0^-, I_0^- stand for the reflected field

Since $\frac{V_0^+}{I_0^+} = -\frac{V_0^-}{I_0^-} = Z_0$

we have

$$V(z) = V_0^+ e^{-z\gamma} + V_0^- e^{z\gamma} \quad (3)$$

$$I(z) = \frac{V_0^+}{Z_0} e^{-z\gamma} - \frac{V_0^-}{Z_0} e^{z\gamma} \quad (4)$$

at $z=l$, we have $\frac{V(l)}{I(l)} = Z_L$

$$Z_L = Z_0 \frac{V_0^+ e^{-l\gamma} + V_0^- e^{l\gamma}}{V_0^+ e^{-l\gamma} - V_0^- e^{l\gamma}} \quad (5)$$

Meanwhile at $z=l$, we define

$$\Gamma = \frac{V_0^- e^{l\gamma}}{V_0^+ e^{-l\gamma}} \quad \Rightarrow \quad V_0^- = V_0^+ e^{-2l\gamma}\Gamma \quad (6)$$

Using (6) in (5), we have

$$Z_L = Z_0 \frac{1+\Gamma}{1-\Gamma} \quad \text{and} \quad \Gamma = \frac{Z_L - Z_0}{Z_L + Z_0} \quad (7)$$

Using (6) in (3) and (4), we can write

$$V(z) = V_0^+ e^{-l\gamma}(e^{-\gamma(z-l)} + \Gamma e^{\gamma(z-l)}) \quad (8)$$

$$I(z) = \frac{V_0^+}{Z_0} e^{-l\gamma}(e^{-\gamma(z-l)} - \Gamma e^{\gamma(z-l)}) \quad (9)$$

The two measurements we have are

$$V^+(z_1) = V_0^+ e^{-z_1\gamma} \quad (10)$$

$$V^-(z_2) = V_0^- \Gamma e^{-2l\gamma} e^{z_2\gamma} \quad (11)$$

at $z=l$ we have

$$V(l) = V_0^+ e^{-l\gamma} + V_0^- e^{l\gamma} \quad (12)$$

$$I(l) = \frac{V_0^+}{Z_0} e^{-l\gamma} - \frac{V_0^-}{Z_0} e^{l\gamma} \quad (13)$$

Rearranging (12) and (13), we have

$$V(l) = V_0^+ e^{-z_2\gamma} e^{-\gamma(z_1-l)} + V_0^+ \Gamma e^{-2l\gamma} e^{z_2\gamma} e^{-\gamma(z_2-l)} \quad (14)$$

$$I(l) = \frac{1}{Z_0}[V_0^+ e^{-z_1\gamma} e^{-\gamma(z_1-l)} - V_0^+ \Gamma e^{-2l\gamma} e^{z_2\gamma} e^{-\gamma(z_2-l)}] \quad (15)$$

Using (12) and (13) in (14) and (15), we have

$$Z_L = \frac{V(l)}{I(l)} = Z_0 \frac{V^+(z_1)e^{\gamma(z_1-l)} + V^-(z_2)e^{-\gamma(z_2-l)}}{V^+(z_1)e^{\gamma(z_1-l)} - V^-(z_2)e^{-\gamma(z_2-l)}} \quad (16)$$

From (16), we have

$$Y_L = \frac{1}{Z_L} = Y_L^r + jY_L^i \quad (17)$$

For a parallel RLC resonant circuit, Y_L is

$$Y_L = \frac{1}{R} + j(\omega C - \frac{1}{\omega L})$$

$$= \frac{1}{R}[1 + j(\frac{\omega RC\omega_0}{\omega_0} - \frac{RC}{\omega LC})]$$

For a parallel RLC resonant circuit, the resonant frequency ω_0 and quality factor Q_0 are

$$\omega_0 = \frac{1}{\sqrt{LC}} \quad \text{and} \quad Q_0 = RC\omega_0$$

Using these relations to Y_L, we have

$$Y_L = \frac{1}{R}[1 + jQ_0(\frac{\omega}{\omega_0} - \frac{\omega_0}{\omega})] \quad (18)$$

From (18), we have

$$Y_L^r = \frac{1}{R}$$

$$Y_L^i = \frac{Q_0}{R}[\frac{\omega}{\omega_0} - \frac{\omega_0}{\omega}]$$

Since Y_L^r and Y_L^i are derived from (16) and are known for a given frequency, we can use (18) to solve for ω_0, the resonant frequency, if Q_0 is known,

$$\frac{\omega}{\omega_0} - \frac{\omega_0}{\omega} = A, \tag{19}$$

where,

$$A = \frac{RY_L^i}{Q_0}$$

Solving (19) for ω_0, we have

$$\omega_0 = \frac{1}{2}(-A\omega \pm \sqrt{\omega^2 A^2 + 4\omega^2})$$

Since $\omega_0 > 0$, we have

$$\omega_0 = \omega(\sqrt{1 + \frac{A^2}{4}} - \frac{A}{2}) \tag{20}$$

For $Q_0 >> 0$, and $\frac{|\omega - \omega_0|}{\omega_0} << 1$, we have $A << 1$, then (20) becomes

$$\omega_0 - \omega = \Delta\omega \approx -\frac{A\omega}{2} = -\frac{\omega}{2Q_0}\frac{Y_L^i}{Y_L^r} \tag{21}$$

Eq. (21) is used to determine the difference between the resonant frequency , ω_0, and the operation frequency, ω. Notice that the error signal is proportional to the imaginary part of the cavity load admittance.

4 SIMULATION RESULTS

To verify the validity of Eq. (21) together with Eq. (16), a simulation is conducted using Eq. (16) and Eq. (21) to get the error signal vs. frequency. The results are shown in Figure 2.

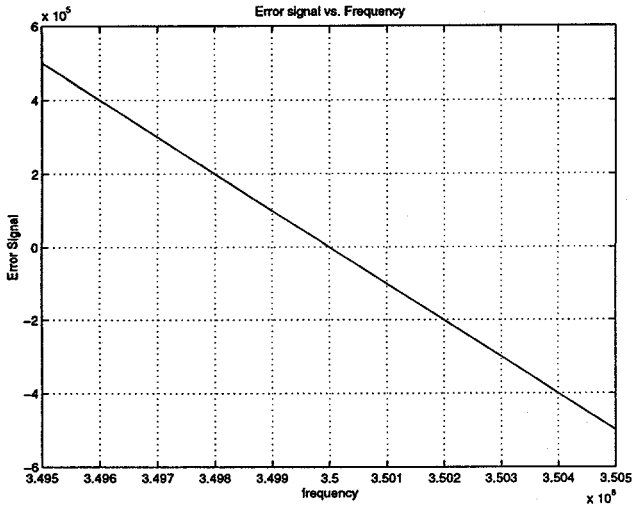

Figure 2. Error signal vs. frequency

In Figure 2, the exact result is shown with a dashed line, but it can not been identified since it is almost the same as the approximate solution. This result shows that Eq. (21) together with Eq. (16) gives satisfactory result within the frequency range we are interested.

Next, we conduct simulations with random noise included the measured forward and reflected field. In figure 2, the correction frequency is obtained when the SNR (Signal-to-Noise Ratio) of the measured field is 20dB. Notice that the perfect gain-matching in our digital I/Q demodulation scheme ensures that the equal effect of noise on both I and Q channels. Thus, we can represent the measured field as $(1+r)F$, where r is noise, F is the complex field without noise. Mathematically, this means that the noise correlation coefficient between two channels (I and Q) is one.

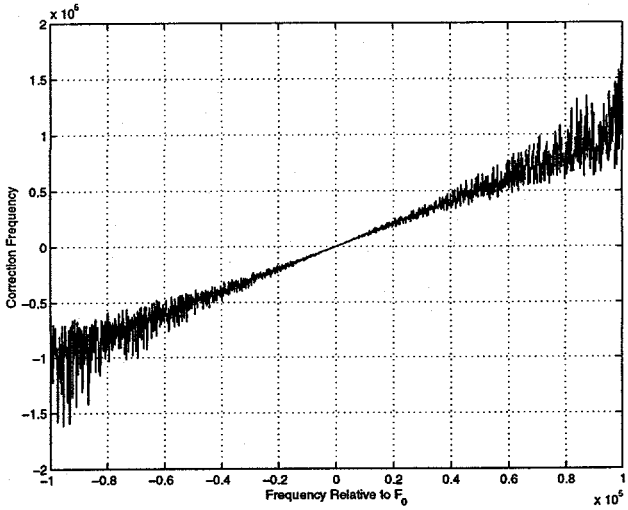

Figure 3. The result with noise in the measurement.

One important feature in Figure 2 is that the correction frequency never cross on both side of the resonant frequency f_0. Next we investigate the correlated and uncorrelated I/Q noise on robustness of the algorithm. Here, we assume that the SNR of the measurement is only 3dB. Figure 4 is for the completely correlated noise. Figure 5 is for the completely uncorrelated noise case. It is very important to notice that the correction frequency never cross zero on both side of the resonant frequency for the case with the completely correlated noise for I/Q components. This means that when we implement this algorithm in this case, we always have a correct sign for the error signal which is very important for not jumping back and forth around the resonant frequency. On the contrast, the error signal for the completely uncorrelated case jumping back and forth across zero on both side of the resonant frequency.

As mentioned before, the digital I/Q decomposition scheme implemented in our system ensures the perfect gain-matching for the I and Q channels which results in

the completely correlated noise for the I and Q channels. Therefore, the algorithm applied to our system is very robust.

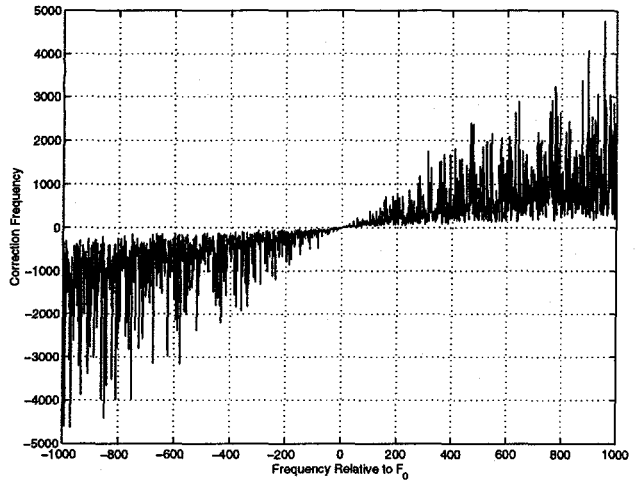

Figure 4. The result for the completely correlated noise with 3dB SNR.

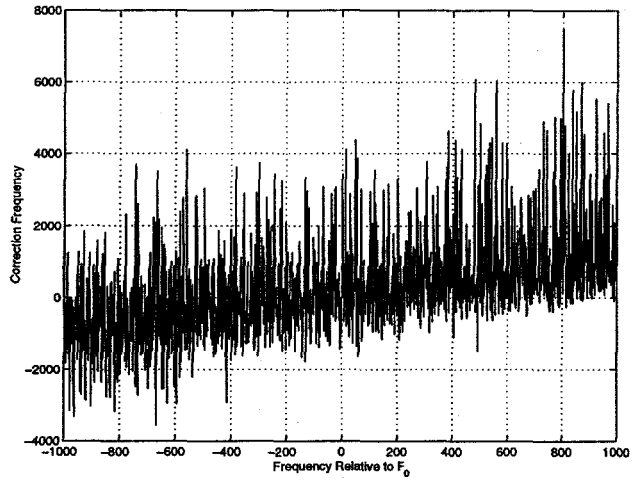

Figure 5. The result for the completely uncorrelated noise with 3dB SNR.

5 OTHER CONSIDERATIONS

Here, all formulas are derived based on the forward and reflected fields. The similar formulas can also be derived from the forward and transmitted fields. Mathematically, they are equivalent. But some practical issues should be addressed when we decide which set of formulas to use in the system implementation. One limitation comes from the finite resolution of A/D converter. For a 12bit A/D converter, as we used in our system, the dynamic range of measurement is around 60dB. However, due to some instrumentation limitations, such as isolation of directional coupler, the dynamic range of measured signal could be 10 to 20 dB lower than the theoretic dynamic range of the A/D converter. Due to above consideration we don't want the magnitude of measured field change dramatically in the normal operation.

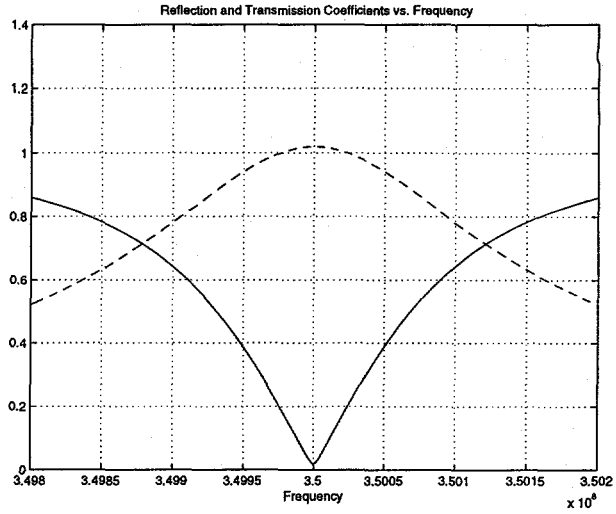

Figure 6. Magnitude of the reflection and transmission coefficients vs. frequency.

Figure 6 depicted the magnitude of the reflection and transmission coefficients for an equivalent RLC load with $Q = 3000$ and $f_0 = 350\,\text{MHz}$. From Figure 6, we can see that using reflected filed algorithm is good when the frequency is relatively away from the resonance but the accuracy of the measurement will deteriorate when the frequency is close to the resonance. However, on the other hand, the accuracy of the transmitted field algorithm is higher when the frequency is close to the resonance and lower when the frequency is away from the resonance. Based on above observation, both algorithms are implemented in our system. The reflected field algorithm will be activated when the frequency is relatively away from the resonance and the transmitted field algorithm will be activated when the frequency is close to the resonance.

6 CONCLUSIONS

An efficient and simple algorithm which is suitable for the implementation in a digital signal processor is proposed. The simulation results reveal that the algorithm is very robust when implemented with the digital I/Q demodulation scheme used in our system. The algorithm gives a good result with a noise level at 20dB SNR.

REFERENCES

[1] Cheng, K.C., 'Field and Wave Electromagnetics', Second Edition, Addison-Wesley, 1989.

[2] Ziomek, C. and Corredoura, P., 'Digital I/Q Demodulator', PAC'95, 1995.